Disentangling Neighbors and Extended Range Density Oscillations in Monatomic Amorphous Semiconductors

S. Roorda,[1,*] C. Martin,[2] M. Droui,[1] M. Chicoine,[1] A. Kazimirov,[3,†] and S. Kycia[2,‡]

[1]*Département de physique, Université de Montréal, 2900 Boulevard Edouard Montpetit, H3C 3J7 Montréal, Québec, Canada*
[2]*Physics department, University of Guelph, 50 Stone Road East, Guelph, Ontario, N1G 2W1, Canada*
[3]*CHESS, Wilson Laboratory, Cornell University, Ithaca, New York 14853, USA*

(Received 2 February 2012; published 20 June 2012)

High energy x-ray diffraction measurements of pure amorphous Ge were made and its radial distribution function (RDF) was determined at high resolution, revealing new information on the atomic structure of amorphous semiconductors. Fine structure in the second peak in the RDF provides evidence that a fraction of third neighbors are closer than some second neighbors; taking this into account leads to a narrow distribution of tetrahedral bond angles, $(8.5 \pm 0.1)°$. A small peak which appears near 5 Å upon thermal annealing shows that some ordering in the dihedral bond-angle distribution takes place during structural relaxation. Extended range order is detected (in both *a*-Ge and *a*-Si) which persists to beyond 20 Å, and both the periodicity and its decay length increase upon thermal annealing. Previously, the effect of structural relaxation was only detected at intermediate range, involving reduced tetrahedral bond-angle distortions. These results enhance our understanding of the atomic order in continuous random networks and place significantly more stringent requirements on computer models intending to describe these networks, or their alternatives which attempt to describe the structure in terms of an arrangement of paracrystals.

DOI: 10.1103/PhysRevLett.108.255501 PACS numbers: 61.43.Dq, 61.05.cp, 81.05.Gc

Much effort, both experimental and theoretical, has been aimed at developing a complete understanding of the atomic structure of amorphous silicon (*a*-Si) and germanium (*a*-Ge). This is fueled by the significant role of *a*-Si as a material with beneficial properties as a solar cell or in microelectronics, and because *a*-Si and *a*-Ge are fundamentally examples of single element covalent bond amorphous semiconductors. Recently, TEM [1], Raman [2], and x-ray scattering [3] in conjunction with carefully prepared samples produced ever more subtle detail to our understanding of the local and intermediate-range structure of this fundamental amorphous system. While in other, less elemental, amorphous materials ordering on an extended length scale has been observed [4], no such ordering has been detected in *a*-Si or *a*-Ge, and the interplay between such extended ordering and structural relaxation is completely unknown.

In this work we present results from high energy x-ray diffraction with high-resolution pair distribution function analyses of as-implanted and annealed amorphous germanium that address both the intermediate (2nd and 3rd neighbors) and extended range ordering.

The short-range order in *a*-Si [5] and *a*-Ge [2,6,7] is believed to approximate a fully fourfold-coordinated continuous random network (CRN). In spite of the close resemblance between short-range order in the crystal and amorphous phases, the intermediate-range order (2nd and 3rd neighbors) is so different that in the radial distribution function (RDF) no clear peak is found at a position corresponding to the 3rd neighbor distance of the crystalline phase. Since the tetrahedral bond is stiff both in bond length and in direction, the lack of order beyond 2nd neighbors must be attributed to a wide distribution in dihedral angles.

Figure 1 displays, schematically, 8 atoms and the bonds between them. The double arrow indicates a tetrahedral angle. The atoms marked "3" are 3rd neighbors of the atom marked "0," and a dihedral rotation (colored arrows) spins atoms "3" around the dashed circle. A uniform distribution of dihedral angles results in a nonuniform distribution of 3rd neighbor distances with relatively sharp peaks near the shortest and longest possible 3rd neighbor distance [6]. Moreover, some of the nearest 3rd neighbors can be closer than some 2nd neighbors. Resolving the structure in the second peak in the RDF due to

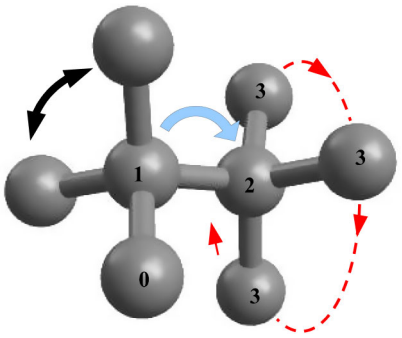

FIG. 1 (color online). Schematic representation of bonding in fourfold-coordinated amorphous semiconductors. Only eight connected atoms are depicted with arrows indicating possible tetrahedral and dihedral bond-angle variations.

 © 2012 American Physical Society

contributions from 2nd and 3rd neighbors requires an experimental resolution of 0.1 Å, which in turn requires a diffraction experiment with a maximum Q range of 30 $Å^{-1}$ or more. In this Letter, we describe the principal results of such an experiment.

Pieces of crystalline Ge (c-Ge) wafers were held at liquid nitrogen temperature and ion implanted with Ge ions (0.5–40 MeV; 0.1–2.5 $\times$ 10^{14} ions/cm^2), resulting in a dense and pure layer of a-Ge extending from the surface to a depth of 10 μm [8]. One sample was annealed under argon for 10 min at 365 °C. The samples were protected by an etch-resistant mask which left an opening, on the backside only, of 5 $\times$ 5 mm^2 at the center of the 4 cm^2 square pieces. A chemical etch removed the c-Ge until only the a-Ge remained in the central area, supported by the surrounding material, thus creating a framed membrane window ideal for x-ray diffraction in transmission geometry. Because of variations in etching speed, the thickness of the membranes as measured by Fourier transform infrared spectroscopy varied from 8.76 to 9.65 μm. Both sides of the sample were analyzed by elastic recoil detection–time of flight [9] which detected no impurities and by Raman spectroscopy which established that the membranes were fully amorphous. Upon initial x-ray measurements, small Bragg peaks were found which varied in intensity as different positions on the samples were probed. The membranes were reimplanted, again at liquid nitrogen temperature, this time from both sides and at ion fluxes not exceeding 100 nA/cm^2 in order to avoid beam heating. After this treatment (and repeating the thermal anneal and the Raman verification) the samples were found to contain no more traces of crystalline remnants giving rise to Bragg peaks.

The x-ray diffraction measurements were carried out at the A2 station of CHESS synchrotron using monochromatic 60 keV x rays and a five-element Ge detector mounted on the 2θ arm of a four-circle Huber diffractometer enabling an accessible Q range up to 55 $Å^{-1}$. The samples were mounted in the vacuum (better than 10^{-5} torr) of a closed cycle helium cryostat and maintained at 10 K during the diffraction experiments. A five-channel lead sheet flight tube with tantalum slits at both ends was used to transport the scattered radiation from the sample to the detector, each element offset by 1.5 mm and therefore covering a small range of 5 different Q values for each diffractometer angle. At each angle of an extensive θ–2θ scan, each detector measured and recorded a full energy spectrum which allowed us to separate the elastic from the Compton scattering.

All experimental data were corrected for background, dead time, polarization, illuminated volume, visible volume, and Compton scattering and divided by the atomic form factor [10]. The $S(Q)$ data (not shown here) are characterized by a complete absence of sharp Bragg peaks and, comparing the curves for as-implanted and annealed a-Ge, are seen to exhibit a slight sharpening upon thermal annealing. The amplitudes of the broad oscillations rapidly decrease with Q but remain visible in the interference function, $Q(S(Q) - 1)$ even beyond 40 $Å^{-1}$. Fourier transforms were applied to the interference functions. In some cases, the points were calculated only for r values that satisfied $r = n\pi/Q_{\max}$ ($n = 1, 2, 3\ldots$), known as sampling [11]. Fourier transformations directly yield the corresponding pair distribution functions $G(r)$ (PDF), and from these one can calculate the radial distribution functions [$J(r)$, RDF] using an average density of ion implanted a-Ge of 0.0435 atoms/$Å^3$ [12].

Figure 2 shows the second peak in the RDF at seven different values of $Q_{\max}$, which is the upper limit in the Fourier transform. Each successive curve has been presented slightly shifted upwards. As $Q_{\max}$ increases, so does the spatial resolution as illustrated by the straight line segments depicting the theoretical resolution $\pi/Q_{\max}$ for each curve. All curves show periodic oscillations which result from the cutoff (termination) at $Q_{\max}$ with a periodicity similar to the spatial resolution. For all curves, except the one at 15 $Å^{-1}$, the main peak near 4 Å is seen to exhibit fine structure and for the last 4 curves, it is clearly observable that two peaks are present. The positions of those two peaks are independent of $Q_{\max}$, and therefore independent of the spatial resolution, as indicated by the vertical line segments drawn at 3.82 and 3.98 Å. Furthermore, the separation between the two peaks becomes clearer as the resolution improves, in contrast to the amplitudes of the termination induced oscillations which decrease for larger $Q_{\max}$. We thus conclude that the asymmetry seen in the second peak is real and not an artifact.

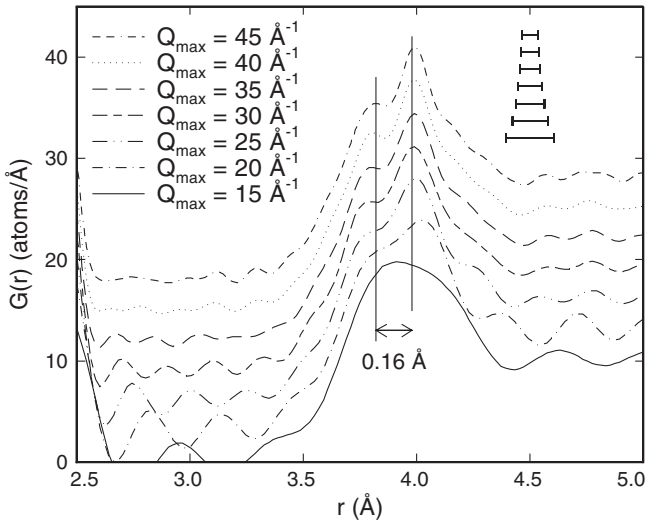

FIG. 2. Second peak in the a-Ge (annealed) RDF for different values of $Q_{\max}$. (Curves have been offset for clarity.) Straight segments in top right corner indicate theoretical resolution for each of the $Q_{\max}$ values. Two straight and parallel vertical lines illustrate increased visibility of fine structure in the second peak.

We compare the RDF of annealed a-Ge (black dots) with a theoretical curve in Fig. 3 The Fourier transformation was executed using exponential damping so as to suppress termination ripples which reduces the spatial resolution, but even so the fine structure in the second peak is still visible as a shoulder on the low-r side of the peak at 4 Å. The theoretical curve is a composite of a Gaussian first peak, a Gaussian representing second neighbors centered at the low-r side of the second peak, a double peaked curve due to third neighbors with a nearly uniform distribution of dihedral angles (as reported for a computer model of amorphous Si [13]) and convoluted to the same width as the second neighbor peak, and a continuously rising curve which is a convolution of the average density and an error function centered near 5 Å. The average density underestimates the contribution of 4th and 5th neighbors leading to the large difference between data and calculation near 5 Å. The Gaussian functions were fit to the data by three-parameter minimization; no attempt was made to optimize the parameters of the other components to the theoretical curve.

From the first peak we conclude that the coordination number $C_1 = 3.68 \pm 0.02$, and the bond length $r_1 = 2.429 \pm 0.001$ Å. The width, with contributions from thermal and static disorder, is 0.057 ± 0.001 Å. The second peak was determined by fitting to the low-r flank of the second peak, to a maximum r of 3.89 Å, and it results in a second neighbor coordination number of $C_2 = 10.2 \pm 0.3$, a second neighbor distance $r_2 = 3.890 \pm 0.006$ Å, and width of 0.223 ± 0.004 Å. These results were stable when the maximum range was varied between 3.81 and 3.92 Å but not beyond. The expected coordination for a random network with $C_1 = 3.68$ would be $C_2 = 9.87 \pm 0.03$ so that the fitted Gaussian peak probably includes a few third neighbors. The static disorder, taking into account the static disorder in r_1, implies a width of the tetrahedral bond-angle distribution of only $\Delta\theta = (8.5 \pm 0.1)°$, which is significantly less than what one would find when fitting a Gaussian to the entire second peak, $(10.1 \pm 0.1)°$. For as-implanted a-Ge, $C_1 = 3.63 \pm 0.03$, and $r_1 = 2.433 \pm 0.001$ Å.

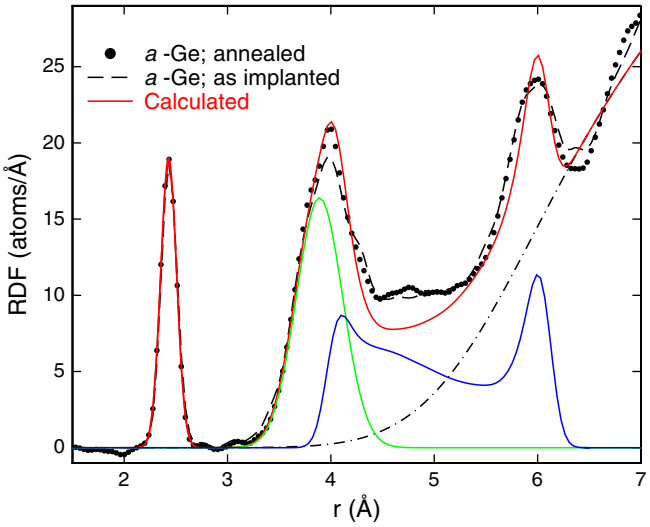

FIG. 3 (color online). Radial distribution function of relaxed a-Ge. Measurement shown as dots (relaxed a-Ge) and dashed line (as-implanted a-Ge). The solid lines correspond to a simple theory where the red line is the sum of a Gaussian centered at the nearest neighbor (not separately shown), a Gaussian centered at the second nearest neighbor distance is shown as a green line, a distribution of third nearest neighbors as discussed in the text (blue line with two peaks near 4 and 6 Å), and a dash-dotted black curve which is a convolution of the average density with an error function.

The agreement and lack thereof between the experimental data and the simple theory provides new and useful information. Clearly, third neighbors contribute to the second peak in the RDF and an unmistakable portion of third neighbors are situated nearer than some *second* neighbors. This implies that only first-principles-based models, which calculate the electron density and permit the identification of covalent bonds between atoms, can be used to identify second and third neighbors. Monte Carlo models relying on distance only to identify second and third neighbors are less adequate in this regard. The first significant deviation between the experimental curve and the simple theory occurs between 4.4 and 5.1 Å, an area that is centered on the third-neighbor distance in the corresponding crystal. This deviation shows that the dihedral angle distribution is not uniform and must include a preferred dihedral angle, not observed in as-implanted a-Ge, between 94° and 135°. Comparing the dots with the dashed line, an increase in dihedral ordering well outside the statistical noise can be seen upon thermal annealing; a similar ordering was suspected to occur in a-Si [5]. Dihedral order peaked at 120° is required for, or evidence of, 6-membered rings. The small difference between as-implanted and relaxed a-Ge seen in Fig. 3 corresponds to 0.13 atoms, which indicates an increase in the number of such rings by 1% (100% corresponds to the number of rings in the fcc diamond structure). To some extent, this ordering seems to support a paracrystalline model, but the behavior on thermal annealing invalidates the interpretation of fluctuation electron microscopy (FEM) observations in terms of such a model [13]. Paracrystalline models do indeed depict more dihedral order than CRN models; however, the FEM shows that the order *decreases* with annealing [14] whereas here we clearly observe an *increase*.

At larger distances, the RDFs for both a-Ge and a-Si show small subtle changes occurring upon thermal annealing: a slight sharpening of peaks and valleys in the RDF at larger distances. The statistical noise in the RDF tends to obscure such subtle changes. In order to bring them out, we reduced the noise using a damped Fourier transform with $Q_{\max} = 40$ Å^{-1} and investigate not the RDF but the PDF which contains the variation about the average density.

Figure 4 shows the extended range part of the PDFs of both as-implanted and annealed a-Ge (top axis), the PDF of (annealed) a-Si, and that of a 100 k atom CRN model simulation [15] (bottom axis). All curves exhibit clearly discernible oscillations even beyond 20 Å. The oscillations are well described by an exponentially damped sine function. Nonlinear curve fitting was employed to extract the characteristic period and decay length of these oscillations. The period of the oscillations is close to 1.33 r_1, which is the height of the characteristic tetrahedron and also the Bragg (111) spacing. Perhaps surprisingly, the period increases upon thermal annealing, in a-Ge from 1.29 ± 0.01 to 1.35 ± 0.01 and in a-Si from 1.18 ± 0.05 to 1.29 ± 0.02 r_1 (note that r_1 remains nearly constant in both materials).

The decay length similarly increases with thermal annealing, from 1.2 ± 0.4 to 1.8 ± 0.3 r_1 in a-Si, and from 1.87 ± 0.11 to 1.89 ± 0.11 r_1 in a-Ge. The decay length can be taken as a quantifier for the state of relaxation of the network, where a larger decay length is indicative of a more homogeneous network. It thus appears that even the as-implanted a-Ge is as relaxed as annealed a-Si. The most relaxed material is annealed a-Ge, which is the only material where the local order leads to observable fine structure in the second peak. Perhaps the larger undercoordination in a-Ge leads to a less overconstrained network which relaxes more easily than a-Si.

The extended range density variations with a period similar to the (111) d spacing could be taken as evidence for paracrystallinity, or perhaps the sine function behavior is an artifact in the data as a consequence of a Fourier transform. However, the bottom curve in Fig. 4 corresponds to the PDF of the "best" CRN model, 100 k atoms large [15]. This model shows the same decaying density oscillation, with a period of 1.20 ± 0.02 r_1 and a decay length of 0.89 ± 0.07 r_1. The mere presence of the oscillations in the PDF of this real-space computer model indicates that they are intrinsic to the random network [16]. The short decay length compared to the values observed in real materials indicates that the model is appropriate for a network even more "unrelaxed" than our as-implanted samples. It would thus be inappropriate to compare model calculations with the experimental data obtained on *relaxed* a-Si or a-Ge; instead one should compare with data obtained on "*as-implanted*" samples.

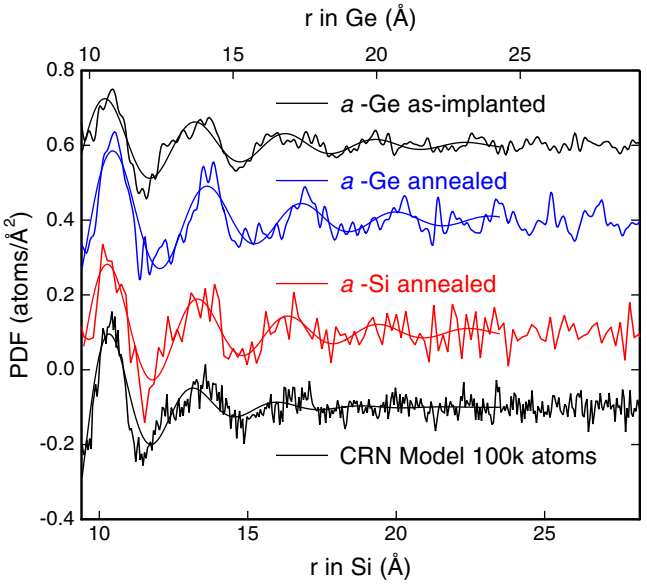

FIG. 4 (color online). Extended range ordering. Pair distribution functions for a-Ge (as-implanted and relaxed), a-Si (relaxed only) [5], and for a theoretical model [15]. Curves have been vertically offset for clarity. Thin lines through each of the experimental curves correspond to nonlinear fits and were used to deduce the periodicity and decay length of the PDFs.

Structural relaxation in amorphous silicon and germanium has been explained in terms of two apparently mutually exclusive mechanisms, namely, bond-angle ordering [17] or defect removal [18]; experimental evidence requires that the average atomic density and the first neighbor distance remain constant to within a fraction of a percent. The present observation that the average tetrahedron is compressed, and relaxes toward the ideal value under thermal annealing in both amorphous Si and Ge, offers a single and compelling scenario for structural relaxation that encompasses both defects and bond angles. Consider five atoms, four of which surround a central atom in a perfect tetrahedron (e.g., atoms 1 and 3 in Fig. 1 surrounding atom 2). By placing three atoms on a base plane and pushing those atoms inward (reducing the radius of the dashed red circle in Fig. 1) while maintaining the interatomic distance, the other two atoms will move straight upwards (to the left of Fig. 1). When the volume of the deformed tetrahedron is thus reduced by 3%, its height is increased from 1.33 to 1.46 bond length but three other "heights" measured with respect to the other three base planes are all reduced to 1.27 bond lengths. At the same time, three of the tetrahedral angles have increased by 8° and three other tetrahedral angles have decreased by 9°. The increase of the average tetrahedron size upon structural relaxation as observed in Fig. 4 therefore implies a local volume expansion and must be accompanied by another mechanism, such as vacancy removal, in order to maintain near-constant average atomic density. The scenario for structural relaxation thus goes as follows: unrelaxed amorphous Si and Ge are continuous random networks with up to a few atomic percent of vacancy-type defects [19] (leading to significantly undercoordinated material) surrounded by material under significant compressive stress (hence the distorted angles and compressed tetrahedrons). Thermal annealing provides atomic mobility as required for defect removal which is accompanied by relaxation of the compressed tetrahedrons towards nearly ideal volumes and a reduction in average bond-angle distortion. It is a testament to the power of RDF-type analysis of high quality data that many elements

of this scenario (bond length, average density, coordination number, average bond-angle distortion, average tetrahedron size and volume, and even defect density [5]) can be deduced directly from the diffraction data.

We thank Louis Godbout and Réal Gosselin for their expert support of the ion implanters, R. Leonelli and G. Bentoumi for assistance with Raman measurements, Xavier Cauchy and Stéphane Lefebvre for assistance with the diffraction measurements, and the CHESS technical staff for their crucial help in developing the multidetector diffractometer and accepting the significant modifications to the fine-tuned A2 wiggler beam line. We gratefully acknowledge G. T. Barkema and N. Mousseau for the coordinates and RDF of the 100 k atom simulation. This work was financially supported by the Fonds de Recherche du Québec–Nature et Technologies through the grant to the Regroupement québécois sur les matériaux de pointe and by the Natural Sciences and Engineering Research Council of Canada. This work is based upon research conducted at the Cornell High Energy Synchrotron Source (CHESS) which is supported by the National Science Foundation and the National Institutes of Health/National Institute of General Medical Sciences under NSF Grant No. DMR-0936384.

*sjoerd.roorda@umontreal.ca
†Deceased.
‡skycia@uoguelph.ca

[1] K. B. Borisenko, B. Haberl, A. C. Y. Liu, Y. Chen, G. Li, J. S. Williams, J. E. Bradby, D. J. H. Cockayne, and M. M. J. Treacy, Acta Mater. **60**, 359 (2012).
[2] C. J. Glover, M. C. Ridgway, K. M. Yu, G. J. Foran, D. Desnica-Frankovic, C. Clerc, J. L. Hansen, and A. Nylandsted-Larsen, Phys. Rev. B **63**, 073204 (2001).
[3] R. Xie, G. G. Long, S. J. Weigand, S. C. Moss, and S. Roorda, J. Non-Cryst. Solids **357**, 2498 (2011).
[4] P. S. Salmon, A. C. Barnes, R. A. Martin, and G. J. Cuello, Phys. Rev. Lett. **96**, 235502 (2006).
[5] K. Laaziri, S. Kycia, S. Roorda, M. Chicoine, J. L. Robertson, J. Wang, and S. C. Moss, Phys. Rev. B **60**, 13 520 (1999).
[6] R. J. Temkin, W. Paul, and G. A. N. Connell, Adv. Phys. **22**, 581 (1973).
[7] G. Etherington, A. C. Wright, J. T. Wenzel, J. C. Dore, J. H. Clarke, and R. N. Sinclair, J. Non-Cryst. Solids **48**, 265 (1982).
[8] M. Droui, M. Sc. thesis, Université de Montréal, 2005.
[9] R. Groleau, S. C. Gujrathi, and J. P. Martin, Nucl. Instrum. Methods Phys. Res. **218**, 11 (1983).
[10] For details of the data handling, see C. M. Martin, M.Sc. thesis, Guelph University, 2010.
[11] R. Lovell, G. R. Mitchell, and A. H. Windle, Acta Crystallogr. Sect. A **35**, 598 (1979).
[12] K. Laaziri, S. Roorda, and J. M. Baribeau, J. Non-Cryst. Solids **191**, 193 (1995).
[13] S. M. Nakhmanson, P. M. Voyles, N. Mousseau, G. T. Barkema, and D. A. Drabold, Phys. Rev. B **63**, 235207 (2001).
[14] J. Y. Cheng, J. M. Gibson, and D. C. Jacobson, J. Mater. Res. **16**, 3030 (2001).
[15] G. T. Barkema and N. Mousseau, Phys. Rev. B **62**, 4985 (2000).
[16] A. C. Wright, Phys. Chem. Glasses, Eur. J. Glass Sci. Technol. B **49**, 103 (2008).
[17] J. S. Lannin, Phys. Today **41**, No. 7, 28 (1988); J. Non-Cryst. Solids **97-98**, 39 (1987).
[18] S. Roorda, W. C. Sinke, J. M. Poate, D. C. Jacobson, S. Dierker, B. S. Dennis, D. J. Eaglesham, F. Spaepen, and P. Fuoss, Phys. Rev. B **44**, 3702 (1991).
[19] S. Coffa, J. M. Poate, D. C. Jacobson, and A. Polman, Appl. Phys. Lett. **58**, 2916 (1991).